J Appl Electrochem (2009) 39:2001–2006
DOI 10.1007/s10800-009-9910-6

ORIGINAL PAPER

# Synthesis, structural, and electrochemical performance of $V_2O_5$ nanotubes as cathode material for lithium battery

**V. M. Mohan · Bin Hu · Weiliang Qiu · Wen Chen**

Received: 8 December 2008 / Accepted: 14 April 2009 / Published online: 29 April 2009


**Abstract** Various vanadium oxide nanostructures are currently drawn interest for the potential applications of Li batteries, super capacitors, and electrochromic display devices. In this article, the synthesis of $V_2O_5$ nanotubes by hydrothermal method using 1-hexadecylamine (HDA) and PEO as a template and surface reactant were reported, respectively. The structural properties and electrochemical performances of these nanostructures were investigated for the application of Li batteries. Structure and morphology of the samples were investigated by XRD, FTIR, SEM, and TEM analysis. The battery with $V_2O_5$ nanotubes electrode showed initial specific capacity of 185 $mAhg^{-1}$, whereas the PEO surfactant $V_2O_5$ nanotubes exhibited 142 $mAhg^{-1}$. It was found that PEO surfactant $V_2O_5$ nanotubes material showed less specific capacity at initial stages but better stability was exhibited at higher cycle numbers when compared to that of $V_2O_5$ nanotubes. The cyclic performance of the PEO surfactant material seems to be improved with the role of polymeric component due to its surface reaction with $V_2O_5$ nanotubes during the hydrothermal process.

**Keywords** $V_2O_5$ nanotube · Poly(ethylene oxide) · Cathode · Electrochemical performance · Li battery

V. M. Mohan · B. Hu · W. Qiu · W. Chen (✉)
State Key Laboratory of Advanced Technology for Materials Synthesis and Processing, and School of Materials Science and Engineering, Wuhan University of Technology, 430070 Wuhan, People's Republic of China
e-mail: chenw@whut.edu.cn

## 1 Introduction

The synthesis of nanosized materials with specific geometry and morphology is a key aspect in various fields such as modern materials [1, 2], biotechnology [3, 4], catalysis [5, 6], electronics [7, 8], and power sources [9, 10]. Particularly, the higher order nanostructures with well defined geometries like nanotubes, nanowires, nanofibers, and nanorods have attracted much attention now a days because of their importance in both fundamental as well as engineering science and potential applications in various nanodevices [11–14]. Vanadium oxides have been extensively investigated as possible cathode materials for lithium batteries.

Vanadium pentoxide ($V_2O_5$) belongs to the transition metal oxides family and is often employed in secondary lithium batteries to improve the specific capacity, voltage (versus the anode material), reversibility, and stability. Previous studies indicated that the diffusion coefficient of $Li^+$ in crystalline $V_2O_5$ is inherently low, i.e., $D_i \sim 10^{-12}$ $cm^2$ $s^{-1}$ [15, 16]. Considering this fact, many researchers concluded that the capacity of lithium intercalation at high discharge rates can be improved by controlling the size and shape of the individual particles and the morphology of the $V_2O_5$ electrode material. Various nanostructures of $V_2O_5$ were already synthesized by a variety of methods and galvanostatic discharge experiments shows that nanostructure electrodes delivered higher capacities than thin film electrodes [17–21].

However, there is another problem which can be solved related to the structural changes. Crystalline $V_2O_5$ undergoes structural modification during deep charge–discharge cycles induced by mechanical stress leading to a decrease in the specific $V_2O_5$ properties such as energy density or charge capacity. These structural modifications generated

from the variety of sources such as volumetric changes due to the electrochemical insertion/extraction of $Li^+$ ion, solvent transport into or out of the material during redox cycling and changes in the coordination geometry at the metal center by the result of redox transition. All these processes lead to detrimental effect on the long-term dimensional stability of the material. Structural changes are accompanied by the loss of conductive pathways within the material which degrade the charge storage capacity and the rate of charge extraction. In order to overcome these problems, the production of nanocomposites and nanostructures materials has been used [22–24]. Nanotubular materials are expected to have unusual characteristics amplified by their marked shape-specific and quantum size effects. The possibility of chemically modifying the outer, inner surfaces and edges also has an advantage to enhance the nanotube characteristics.

In the present article, we synthesized $V_2O_5$ nanotubes and PEO surfactant $V_2O_5$ nanotubes by simple hydrothermal method and its structure is analyzed by XRD and FTIR studies. The dimensions of the nanotubes were determined by SEM and TEM analysis. The battery performance was estimated by the cyclic voltagramms and discharge curves.

## 2 Experimental

### 2.1 Synthesis of vanadium oxide nanotubes

In the synthesis of vanadium oxide nanotubes, 10 mmol $V_2O_5$ (99.5%) was added 10 mmol 1-hexadecylamine (Acros Crganics Company) and 20 mL distilled water and the resulting solution was stirred for 1 h. After 1 h, another 20 mL distilled water was added. This solution was allowed to hydrolyze under vigorous stirring for 48 h at room temperature. Then this mixture solution was poured into a Teflon-lined autoclave with a stainless steel shell and treated hydrothermally at 180 °C for 7 days. The precipitate was washed with absolute alcohol and then with distilled water and allowed it at 80 °C for 5 h. In order to prepare the polymer surface reactant $V_2O_5$ nanotubes the above procedure was repeated with the addition of 0.5 mol% PEO to the vanadium oxide–amine mixture.

### 2.2 Preparation of Li batteries

Electrochemical batteries were assembled in a dry glove box filled with an argon gas using lithium pellets as negative electrode, 1 M solution of $LiPF_6$ in ethylene carbon (EC)/dimethyl carbonate (DMC) as electrolyte, and pellets made of the obtained products, acetylene black, and PTFE in a 6:4:1 ratio as the positive electrode.

### 2.3 Characterization

The X-ray powder diffraction (XRD) measurement was performed on a D/MAX-III X-ray diffractometer with Cu-K$\alpha$ ($\lambda = 1.5418$ Å) radiation and graphite monochromator. Fourier-transform infrared (FTIR) absorption spectra were recorded using the 60-SXB IR spectrometer with a resolution of 4 $cm^{-1}$. SEM images were obtained using JSM-5610LV scanning electron microscope at 20 kV. TEM images were taken in a JEOL JEM- 2010 FEF microscope operated at 200 kV. Electrochemical studies were investigated by an Autolab Potentiostat 30 System with the scan rate of 0.5 mV $s^{-1}$ at 1.5–4.0 V versus Li/$Li^+$ potential range and a Battery Testing System (BTS-5V/5mA) with the constant current density of 20 $mAg^{-1}$ at 2.0–4.0 V versus Li/$Li^+$ potential range.

## 3 Results and discussions

### 3.1 X-ray diffraction

The X-ray diffraction patterns of $V_2O_5$ nanotubes, 0.5 mol% PEO surfactant $V_2O_5$ nanotubes are shown in Fig. 1. From the XRD patterns, it is clear that the nanotubes and PEO surfactant nanotubes exhibited similar and strongest peaks at (001) (002) (110) (210), and (310), where the structure is preserved. No peaks of any other phases or impurities were observed, demonstrating that $V_2O_5$ nanotubes with high purity could be obtained using the present synthesis process whereas the PEO worked as a surface reactant [25]. No peaks related to polymers were observed in the XRD pattern of PEO surfactant $V_2O_5$ nanotubes.

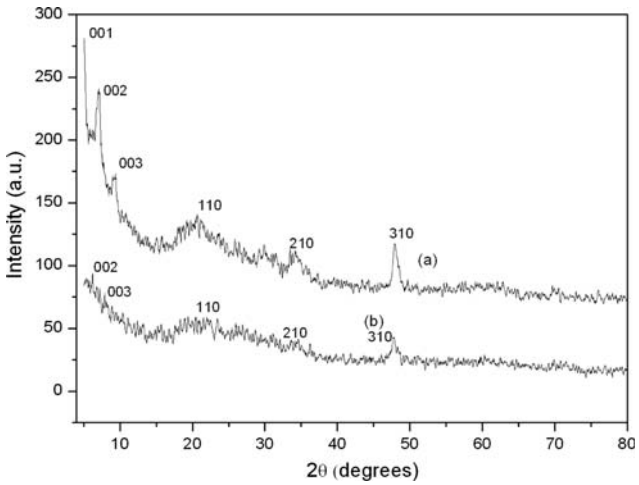


**Fig. 1** XRD patterns of **a** $V_2O_5$ nanotubes and **b** PEO surfactant $V_2O_5$ nanotubes

### 3.2 Fourier transforms infrared radiation (FTIR) spectra analysis

The FT-IR spectra of $V_2O_5$ nanotubes and PEO surfactant $V_2O_5$ nanotubes were shown in Fig. 2. The strong absorption peaks at 2,956, 2,918, 2,850, and 1,468 $cm^{-1}$, which could be assigned to the stretching and bending modes of the different C–H vibrations in the hexadecylamine template, respectively [26]. These bands are also appeared in the same wavelength region as in the PEO surfactant $V_2O_5$ nanotubes. Two absorption bands appeared at 3,414 and 1,646 $cm^{-1}$, could be attributed to the stretching and bending modes of O–H vibrations, respectively. This is exhibited the intercalation of water molecules into the $V_2O_5$ nanotubes layers [26]. Absorption bands between 400 and 1,000 $cm^{-1}$ could be indexed to various (group) vibrations of V–O type [26]. There are three major bands $\nu_s$ (V=O), $\nu_s$ (V–O–V), and $\nu_{as}$ (V–O–V) appeared at 1,005, 574, and 487 $cm^{-1}$ in $V_2O_5$ nanotubes and are shifted to 999, 574, and 500 $cm^{-1}$ that of PEO surfactant $V_2O_5$ nanotubes. The vibration modes ($\nu_s$ and $\nu_{as}$) shifting exhibited oxidation and reduction states of the vanadium oxide ($V^{4+} \leftrightarrow V^{5+}$), respectively [27].

### 3.3 Scanning electron microscopy (SEM) analysis

Figure 3 shows the scanning electron microscopic images of $V_2O_5$ nanotube, PEO surfactant $V_2O_5$ nanotubes uniformly distributed and clearly visible. Vanadium oxide nanotubes are frequently grown together and separately. For the PEO surfactant nanotubes materials interestingly found that the tubes are frequently grown together and are formed as bundles. From the SEM images the length and diameter of the nanotubes are found to be 0.6–1.7 μm and 100–200 nm, respectively.

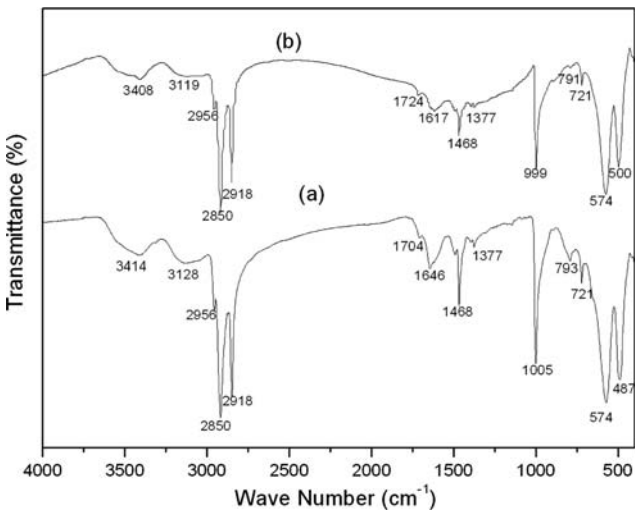


**Fig. 2** FTIR spectra of **a** $V_2O_5$ nanotubes and **b** PEO surfactant $V_2O_5$ nanotubes

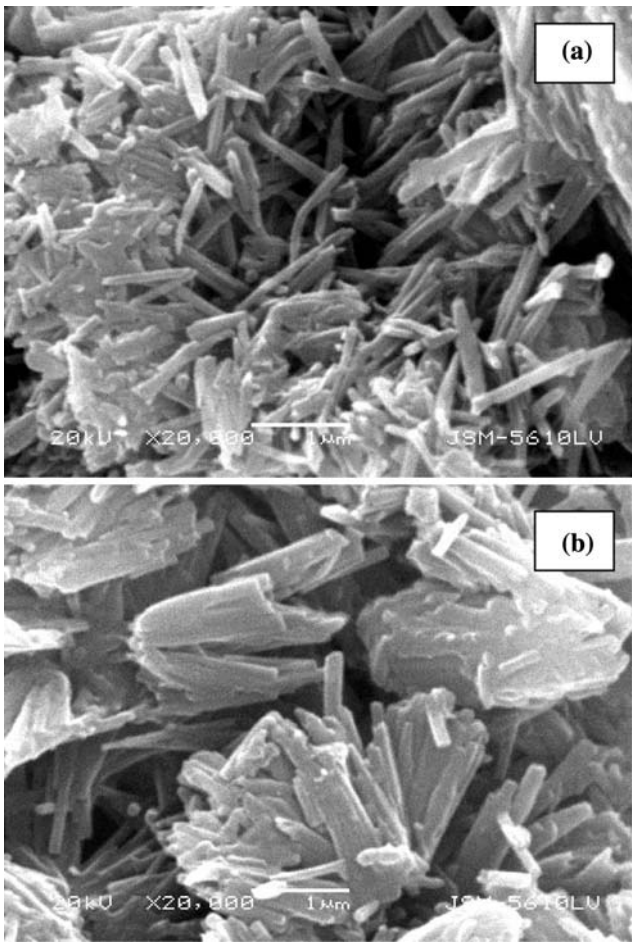


**Fig. 3** SEM images of **a** $V_2O_5$ nanotubes and **b** PEO surfactant $V_2O_5$ nanotubes

Figure 4 shows TEM images of $V_2O_5$ and PEO surfactant $V_2O_5$ nanotubes. From Fig. 4b inner, outer diameters, and crystal lattice distances are found to be 11.64, 54, and 3.325 nm, respectively. According to TEM images there are no significant changes on the diameters and lattice distances due to PEO effect.

### 3.4 Electrochemical investigation

#### *3.4.1 CV analysis*

Figure 5 shows the cyclic voltagrams of $V_2O_5$ nanotubes and PEO surfactant $V_2O_5$ nanotubes, in which the first to tenth cycle curves were plotted. The area $A_i$ ($i$ is the cycle number) is surrounded by each cycle curve represents the amount of the $Li^+$ ions insertion. The cycle efficiency is calculated by the following equation:

$$Q_i = A_i/A_1$$

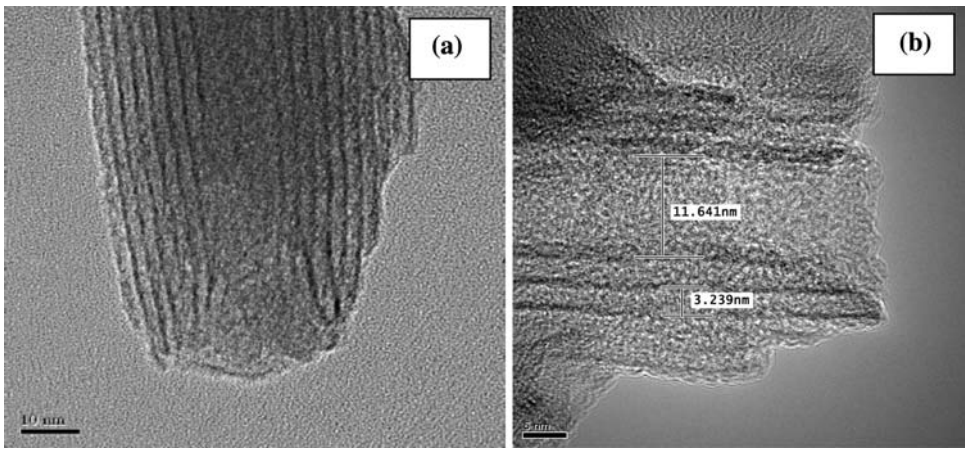


**Fig. 4** TEM images of **a** $V_2O_5$ nanotubes and **b** PEO surfactant $V_2O_5$ nanotubes

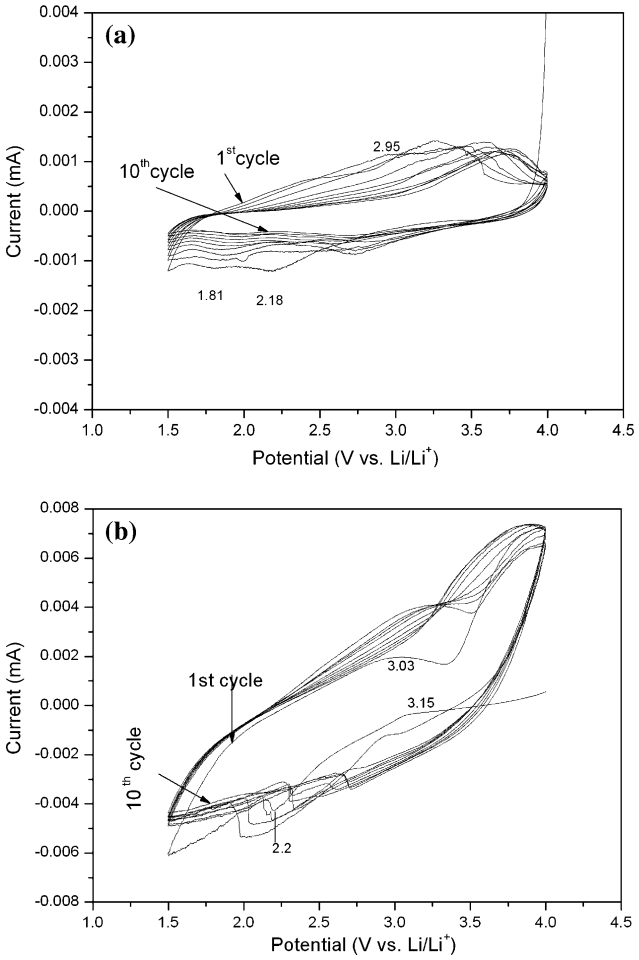


**Fig. 5** Cyclic voltammograms of **a** $V_2O_5$ nanotubes and **b** PEO surfactant $V_2O_5$ nanotubes at the first 10 cycles

where $Q_i$ cycle efficiency, $A_1$ the area of the first cycle curve, and $A_i$ the area of the $i$ cycle curve. The cycle efficiencies of different cycles for $V_2O_5$ and PEO surfactant $V_2O_5$ nanotubes were listed in Table 1. The third cycle efficiency ($Q_3$) of the $V_2O_5$ nanotube and PEO surfactant $V_2O_5$ nanotubes were found to be 94.6 and 96.8%, respectively. Meantime, the tenth cycle ($Q_{10}$) efficiency of $V_2O_5$ nanotube and the PEO surfactant $V_2O_5$ nanotubes were found to be 74.8% and 85.6%, respectively. These results indicate that the cyclic stability of PEO surfactant $V_2O_5$ nanotubes increased when compared to that of $V_2O_5$ nanotubes. Two cathodic current peaks appeared at the potentials of 2.20, 3.15 V and one anodic peak appeared at 3.03 V in the first cycle curve of the PEO surfactant $V_2O_5$ nanotubes (Fig. 5b). These peaks were assigned to the insertion/extraction of $Li^+$ ions between the layers of PEO surfactant $V_2O_5$ nanotubes. In addition, the peaks were shifted with increasing cyclic number suggesting some irreversible $Li^+$ ion interaction between in the PEO surfactant $V_2O_5$ nanotubes [28]. However, there is peak appeared at 3.03 V in the anodic polarization indicated the lithium ions are simultaneously extracted from the $V_2O_5$ layers. It was found that the first and tenth cycles also exhibits both cathodic and anodic peaks indicating that the reversibility of insertion/extraction of $Li^+$ ions in the PEO surfactant $V_2O_5$ nanotubes has been improved. The first cycle of $V_2O_5$ nanotubes showed two peaks at 1.81 and 2.18 V in the cathodic polarization process (Fig. 5a), corresponding to the two different process of $Li^+$ ions. These two peaks could be attributed to the insertion of lithium ions into the $V_2O_5$ nanotubes. However, one obvious peak observed at 2.95 V in the anodic polarization and is completely disappeared with increasing cyclic number indicates that poor cyclic performance of battery made of $V_2O_5$ nanotubes cathode. The different cyclic efficiencies were

**Table 1** The cyclic efficiency of the materials at different cycles

| Material | $Q_3$ | $Q_6$ | $Q_{10}$ |
|---|---|---|---|
| $V_2O_5$ nanotubes | 94.6 | 87.3 | 74.8 |
| PEO surfactant $V_2O_5$ nanotubes | 96.8 | 92.6 | 85.6 |

shown in Table 1. Similar types of results were also observed in PEO mixed $MoO_3$ nanomaterial [29].

### 3.5 Battery discharge characteristics

Figure 6 shows the curves of discharge capacity versus the cycle number for the electrodes made of $V_2O_5$ nanotubes and PEO surfactant $V_2O_5$ nanotubes with charge–discharge current density 21.86 $mAg^{-1}$ at 25 °C. The initial specific charge capacity 185 $mAhg^{-1}$ of the $V_2O_5$ nanotubes was already reported in our group [30]. The discharge curves showed a multistep process due to its structural changes upon the $Li^+$ ions insertion/extraction process [31]. The specific capacity increasing in the second cycle of pure $V_2O_5$ nanotubes compared to that of first cycle is likely due to the film cracking caused by the first cycle. The cracking or defects in the films after first cycle allows more freedom for volumetric charge during Li-ion insertion/extraction, and thus the capacity increases in the second cycle [28]. The discharge capacity of PEO surfactant $V_2O_5$ nanotubes is found to be 142 $mAhg^{-1}$ in the first cycle, which is lower than that of $V_2O_5$ nanotubes. It was decreased slowly and its capacity retains 95 $mAhg^{-1}$ after fifteenth cycles corresponding to 66.9% of its initial capacity. The decreasing capacity in the PEO surfactant $V_2O_5$ nanotubes battery might be due to decrease in average vanadium oxidation state. The discharge capacity of PEO surfactant $V_2O_5$ nanotubes showed less in the lower cyclic number and it exhibits better after tenth cyclic number compared to that of $V_2O_5$ nanotubes. In our present investigation, we observed the battery discharge stability increases may be due to the increasing of $Li^+$ ion insertion/extraction into the PEO surfactant $V_2O_5$ nanotubes.

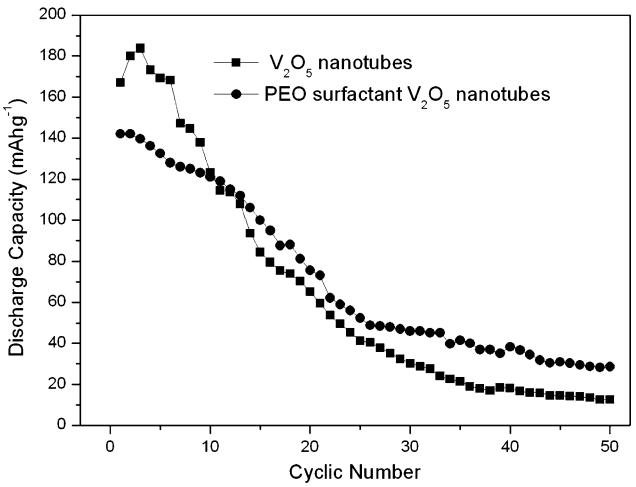


**Fig. 6** Cycling property of $V_2O_5$ nanotubes and PEO surfactant $V_2O_5$ nanotubes at the first 50 cycles

## 4 Conclusions

A simple hydrothermal method was introduced for the preparation of $V_2O_5$ nanotubes and PEO surfactant $V_2O_5$ nanotubes. The XRD patterns and FTIR spectra reveals that there is no large influence on the crystal structure of $V_2O_5$ by using of PEO. From the SEM image it was clear that the PEO surfactant $V_2O_5$ nanotubes were grown in the form of bundles. From the TEM images the inner, outer diameters, and crystal lattice distances were found to be 11.64, 54, and 3.325 nm, respectively. The cyclic voltagrams indicate that the PEO surfactant $V_2O_5$ nanotubes has better cyclic stability than that of $V_2O_5$ nanotubes. The $V_2O_5$ nanotubes electrode battery showed initial specific capacity 185 $mAhg^{-1}$, whereas the PEO surfactant $V_2O_5$ nanotubes exhibited 142 $mAhg^{-1}$ with constant current density of 20 $mAg^{-1}$ at 2.0–4.0 V versus $Li/Li^+$ potential range. The electrochemical tests of PEO surfactant $V_2O_5$ nanotubes showed better stabilized capacity after tenth cycle number compared to that of $V_2O_5$ nanotubes due to its surface reaction.

**Acknowledgements** One of the authors (V. M. Mohan) wishes to thank the Wuhan University of Technology Management for the financial support in the form of Post Doctoral Fellowship. This work is supported by China postdoctoral Science Foundation (CPSF No. 20080440966), National Nature Science Foundation of China (no. 50672071) and the Program for Changjiang Scholars and Innovative Research Team in University, Ministry of Education, China (PCSIRT) (No. IRT0547).

## References

1. Lemon BI, Crooks RM (2000) J Am Chem Soc 122:12886
2. Loscertales IG, Barrero A, Guerrero I, Cortijo R, Marquez M, Ganan-Calvo AM (2002) Science 295:1695
3. Kurth N, Renard E, Brachet F, Robic D, Guerin P, Bourbouze R (2002) J Polymer 43:1095
4. Caruso F, Schuler C (2000) Langmuir 16:9595
5. Ohde H, Wai CM, Kim H, Kim J, Ohde M (2002) J Am Chem Soc 124:4540
6. Poizot P, Laruelle S, Grugeon S, Dupont L, Tarascon JM (2000) Nature 407:496
7. Sau TK, Pal A, Pal T (2001) J Phys Chem B 105:9266
8. Wuelfing WP, Green SJ, Pietron JJ, Cliffel DE, Murray RW (2000) J Am Chem Soc 122:11465
9. Vullum F, Teeters D (2005) J Power Sources 146:804
10. Long JW, Dunn B, Rolison DR, White HS (2004) Chem Rev 104:4463
11. Xia BY, Yang PY, Sun Y, Wu Y, Mayers B, Gates B, Yin Y, Yan H (2003) Adv Mater 5:15
12. Duan XF, Lieber CM (2000) J Am Chem Soc 122:188
13. Pan ZW, Dai ZR, Wang ZL (2001) Science 291:1947
14. Kim GT, Muster J, Krstic V, Park JG, Park YW, Roth S, Burghard M (2000) Appl Phys Lett 76:1875
15. McGraw JM, Bahn CS, Parilla PA, Perkins JD, Readey DW, Ginley DS (1999) Electrochim Acta 45:187
16. Watanabe T, Ikeda Y, Ono T, Hibino M, Hosoda M, Sakai K, Kudo T (2002) Solid State Ionics 151:313

17. Gu G, Schmid M, Chiu PW, Minett A, Fraysse J, Kim GT, Roth S, Kozlov M, Munoz E, Baughman RH (2003) Nat Mater 2:316
18. Pinna N, Wild U, Urban J, Schlogl R (2003) Adv Mater 15: 329
19. Liu J, Wang X, Peng Q, Li Y (2005) Adv Mater 17:764
20. Takahashi K, Wang Y, Cao G (2005) J Phys Chem B 109:48
21. Patrissi CJ, Martin CR (1999) J Electrochem Soc 146:3176
22. Huguenin F, Torresi RM, Buttry DA (2002) J Electrochem Soc 149:A546
23. Malta M, Louarn G, Errien N, Torresi RM (2003) Electrochem Commun 5:1011
24. Murugan AV (2005) Electrochim Acta 50:4627
25. Subba Reddy ChV, Walker EH, Williams QL, Kalluru RR (2009) Curr Appl Phys (in press)
26. Sediri F, Gharbi N (2007) J Phys Chem Solids 68:1821
27. Subba Reddy ChV, Mho S-i, Kalluru RR, Williams QL (2008) J Power Sources 179:854
28. Wang Y, Cao G (2006) Electrochim Acta 51:4865
29. Mai L-Q, Chen W, Xu Q, Zhu Q-Y (2003) J Microelectron Eng 66:199
30. Chen W, Mai L-Q, Qi Y, Dai Y (2006) J Phys Chem Solids 67:896
31. Subba Reddy ChV, Walker EH Jr, Chen W, Mho S-i (2008) J Power Sources 183:330